

60 GHz Circular Patch-Fed High Gain Transparent Lens Antenna

Z. Briqech¹, A. R. Sebak¹, and T. Denidni²

¹Electrical and Computer Engineering Department
Concordia University, 1455 de Maisonneuve West, EV005.127, Montréal, Québec, H3G 1M8, Canada
z_briqec@encs.concordia.ca, abdo@ece.concordia.ca

²Institut National De La Recherche Scientifique (INRS)
Place Bonaventure, 900 De la Gauchetière Ouest, Niveau C, Montréal, Québec, H5A 1C6, Canada
denidni@emt.inrs.ca

Abstract — A high gain, low cost and easy to fabricate millimeter-wave (MMW) antenna is presented. To focus the radiation into a very thin main beam, a concept based on employing a cylindrical air cavity with a convex front-end linking a microstrip patch radiator and a transparent dielectric lens is introduced. This principle is applied to enhance the coupling between the patch antenna and dielectric lens at 60 GHz. The design shows very directive and stable radiation patterns in both the E and H-planes. The proposed antenna exhibits a measured gain of 20 dB over the ISM-band, as well as high radiation efficiency (greater than 90%). The performance of the proposed antenna makes it a promising solution for various MMW applications, including short distance wireless communications and MMW imaging.

Index Terms — Dielectric lens, high gain, millimeter-wave antenna, unlicensed 60 GHz band.

I. INTRODUCTION

Due to the increasing demand for high data rate wireless communications, there has been considerable interest in the development of prototype systems for the 60 GHz unlicensed band. This band is free of charge and utilized in industrial, scientific and medical (ISM) applications. However, due to the resonance of the oxygen molecule absorption in the air, the attenuation loss at 60 GHz exceeds 13 dB/km [1]. This attenuation may limit wireless communication system's transmission range capability.

Recently, integrated lens antennas have been

used successfully in millimeter and sub-millimeter wave applications, such as mm-wave imaging systems [6], traffic collision avoidance devices [7], radio astronomy [8], and satellite communications [9]. A lens works as a focusing system when fed by conventional elements, such as horns, waveguides or microstrip antenna. The lens antenna is thus a technique which can be implemented to increase the antenna gain by focusing the radiated energy [10,11]. Furthermore, there are alternative techniques for increasing the gain of an antenna [2,3,4,5], such as the leaky wave antenna presented as a hybrid microstrip antenna array [12] proposed to operate at MMW antenna. A discrete lens antenna is employed as linear and circular polarization transmit-arrays operating at 60GHz with an average gain of 20 dB presented in [13]. This antenna achieves a power efficiency of 50-61%, which is low compared for example to feed horn antennas. This drawback in efficiency is due to loss associated with discrete lens.

Various lens shapes for antenna applications have been investigated over the years. For instance, spherical, elliptical and extended hemispherical profiles are integrated with planar substrates, [11,12,14,21,22]. Lens designs are governed by geometrical optics (GO) laws [23]. A cylindrical air cavity integrated with a lens antenna operating at 28 GHz was introduced in 2012 [15]. It has a reduced lens size, although the flat end of this air cavity is less efficient in reducing internal reflections. In addition, from a fabrication point of view, certain lens shapes, such as hyper hemispherical or elliptical lenses, are more challenging and the

complexity of the fabrication procedure increases the cost.

High attenuation loss associated with millimeter-wave (MMW) propagation could be compensated for using high-gain antennas such as large-aperture antennas and array structures [20]. However, in MMW applications lens antennas are preferred for their small size and for the ease with which they can be mounted on and integrated with circuits and devices [7,8,22]. In addition, dielectric lenses have highly directive antenna patterns and thermal stability, and are compatible with suppressing surface-wave losses and capable of multiple-beam feeding. Furthermore, lens antennas have wideband capabilities depending on the feeding antenna's bandwidth.

In this paper, the proposed antenna consists of a full spherical dielectric lens, which is usually inexpensive and easier to manufacture than hyper hemispherical and elliptical lenses. The dielectric spherical lens is fed by a single element, a circular patch antenna, and supported by a cylindrical air cavity. To our best of knowledge, this work is the first one investigating the effect of a convex-shaped lens mounted on the top side of the air cavity as a key design parameter of the proposed antenna. This convex shape collimates the beam in order to obtain a more concentrated radiation from the patch antenna compared to those from an extended hemispherical lens with or without an air cavity [15]. Thus, the proposed design with a cylindrical air cavity increases the pencil beam directivity, enhances the antenna radiation characteristic, and improves antenna efficiency.

The proposed antenna achieved 20 dB gain while maintaining high efficiency by utilizing only one radiated element. Using arrays to increase the gain has a drawback in the overall antenna efficiency due to the losses caused by the feeding network [13]. In general, 60 GHz antennas are proposed for short range wireless applications [18]. For instance, this frequency band offers the opportunity of developing new industrial applications; short-range radar, high-resolution target detection, classification, miners wireless communications and tracking, and imaging detection systems. As demonstrated in [19] using real mining environment, 60 GHz antennas, including the proposed antenna, are adequate to

work in the mining industry.

II. ANTENNA GEOMETRY

A. Antenna element

The proposed geometry consists of three components: a lens, the air-cavity, and a microstrip patch antenna, as illustrated in Fig. 1. The spherical dielectric lens antenna is fed by a circular microstrip patch with radius $r_p = 0.78$ mm. The patch is etched on a thin Rogers RT Duroid 5880 ($h_p = 0.254$ mm, $\epsilon_{rL} \approx 2.2$, $\tan\delta \approx 0.0009$) substrate. It is aperture-coupled by a resonant slot with length $L_s = 0.835$ mm and \times width $W_s = 0.1524$ mm. This rectangular radiating slot has an approximate length of $\lambda_g/4$, where λ_g is the guided wavelength at 60 GHz. The slot was drilled with offset from the center of the patch by $d = 0.3$ mm; this distance can be tuned to ensure that the optimum energy of TM_{010} excitation mode is passed through the feed line to the circular patch antenna. The microstrip feed line sits on the back side of the second thin layer composed of Rogers RT Duroid 6010 ($h_f = 0.254$ mm, $\epsilon_{rf} \approx 10.2$, $\tan\delta \approx 0.0023$), which excites the patch via a resonant slotted ground plane. The microstrip patch, feed line and ground plane are simulated as glossy copper sheets of thickness $t = 0.035$ mm with a conductivity of $\sigma = 5.80 \times 10^7$ S/m.

B. Lens configurations

Figure 1 (c) shows the dielectric lens model. The spherical lenses have the advantage of a multi-beam option, which gives them the ability to simultaneously collect signals from all directions. Another advantage is their ability to be manufactured with inexpensive dielectric materials and without the need for active elements. The spherical lens is a homogeneous dielectric sphere [23] which, for dielectric constants in the range $1 \leq \epsilon_{rL} \leq 4$, focuses paraxial rays to a focal point (the radiated element) outside the sphere. The distance F of the focal point from the centre of a lens with radius r_L , and dielectric constant ϵ_{rL} , is approximately determined by geometrical optics (GO) and is given by:

$$F = \frac{r_L \sqrt{\epsilon_{rL}}}{2(\sqrt{\epsilon_{rL}} - 1)}. \quad (1)$$

The lens was selected with same characteristics as those of RO5880. The optimum diameter of the dielectric spherical lens antenna was chosen to be

$D_L = 2 \times r_L = 20 \text{ mm} = 4 \times \lambda_o$ (λ_o is the wavelength in free space) at the central frequency, 60 GHz.

C. Air cavity design

The cylindrical air cavity surrounding the circular patch antenna has important features for enhancing antenna performance. The proposed air cavity resonates at a slightly different frequency than that of the patch antenna, which increases the multi resonances surrounding the main resonance at 60 GHz. This leads to improving the antenna bandwidth as well as potential reduction of the surface-wave interactions in an array environment by isolating each antenna element. Furthermore, the cylindrical shape of the air cavity offers several advantages. One advantage is to guide the near-field propagating wave into the antenna lens, which enhances the directivity and increases the gain of the antenna without a loss in radiation efficiency. Another advantage is that the circular shape of the top of the cavity forms a perfect match to mount the spherical lens antenna. In addition, the top of the air-cavity is covered with the convex lens shape which creates more focusing of the radiated waves that come from the patch antenna, and the optimized dimension of the air cavity maintains the

patch antenna at the focal point.

The cylindrical hole of the proposed air cavity is drilled on a Rogers RT Duroid 5880 ($h_k = 1.575 \text{ mm}$, $\epsilon_{rL} \approx 2.2$, $\tan\delta \approx 0.0009$) substrate with a size $W_k \times L_k = 10.5 \times 9.872 \text{ mm}^2$. The starting design point for the radius (r_k) and height (h_k) of the cylindrical air cavity depends on the focal point distance (F) and the space between the lens end surface and the patch antenna, d_L . In Fig. 1 (c), the aperture angle to the air-cavity edge (ϕ_k) is described by:

$$\phi_k = \sin^{-1}(r_k/r_L). \quad (2)$$

The distance from the center of the lens to the edge of the cavity (d_o) is described by:

$$d_o = \sqrt{r_L^2 - r_k^2}. \quad (3)$$

This leads to determining the lens inset distance into the air-cavity, $d_k = r_L - d_o$, and $d_L = h_k - d_k - t$, where the copper thickness t is taken into account in particular at MMW frequencies. Thus, the focal point is determined as $F = r_L + d_L$ by substituting F in equation (1). d_L is expressed by equation (4), which considers the theoretical GO value as the initial value to determine the approximate focal point at the patch antenna level:

$$d_L = \frac{r_L \sqrt{\epsilon_{rL}}}{2(\sqrt{\epsilon_{rL}} - 1)} - r_L. \quad (4)$$

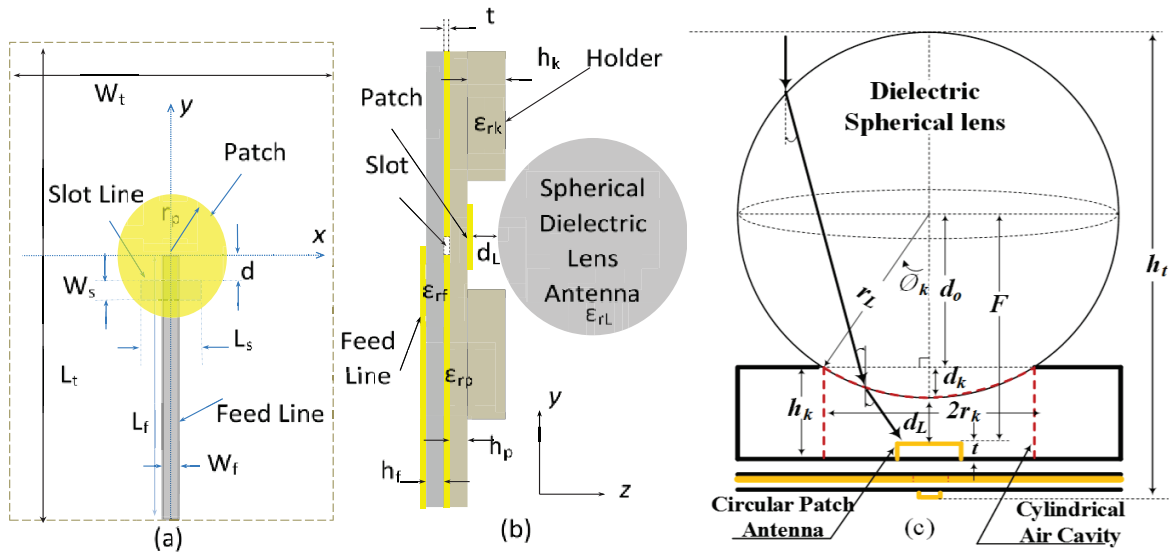


Fig. 1. Antenna geometry: (a) top view, (b), side view, and (c) side view of the proposed antenna.

III. SIMULATION RESULTS

The proposed antenna was studied numerically using the commercial electromagnetic simulator

CST Microwave Studio® (CST-MWS). The model was simulated to investigate the effect of different design parameters and their performance at

operating frequencies from 55 GHz to 65 GHz.

A. Parametric study

1. Cylindrical air cavity design effects

In this study, the aim is to increase the overall antenna gain while keeping a low antenna profile, which reduces the radius of the spherical lens without affecting the broadside directivity. This is accomplished by modeling an optimal combination of the radius and height of the air cavity. For this purpose, a CST model for the patch and air cavity is investigated. As shown in Fig. 2 (a), when the radius of the cavity (r_k) is increased from 1 mm to 4 mm, there are significant changes in the antenna gain, and the resonant frequency goes up. When the radius is close to that of the circular patch (1 mm), the reflected field caused by the cavity is very high

and causes drops in the antenna gain. Also, in form $r_k \geq \lambda_g$ the cavity has a close response to the patch antenna which adds to the overall gain.

The reflection coefficient and antenna gain results are shown in Fig. 2 (b) when the height of the cylindrical air cavity, h_k is changed. The return loss response shifted slightly upwards when the height of the cavity was increased. Furthermore, a higher antenna gain was obtained at $h_k = 1.575$ -mm, with no major influence on the antenna impedance bandwidth. Therefore, $h_k \sim \lambda_g/2$ in the substrate and $r_k \sim \lambda_g$ were the values selected to obtain a good match between the patch and the lens, which is very important in order to optimize the plane-wave radiation of the lens. In addition, these values match the optimum focal point of this model's selected lens material.

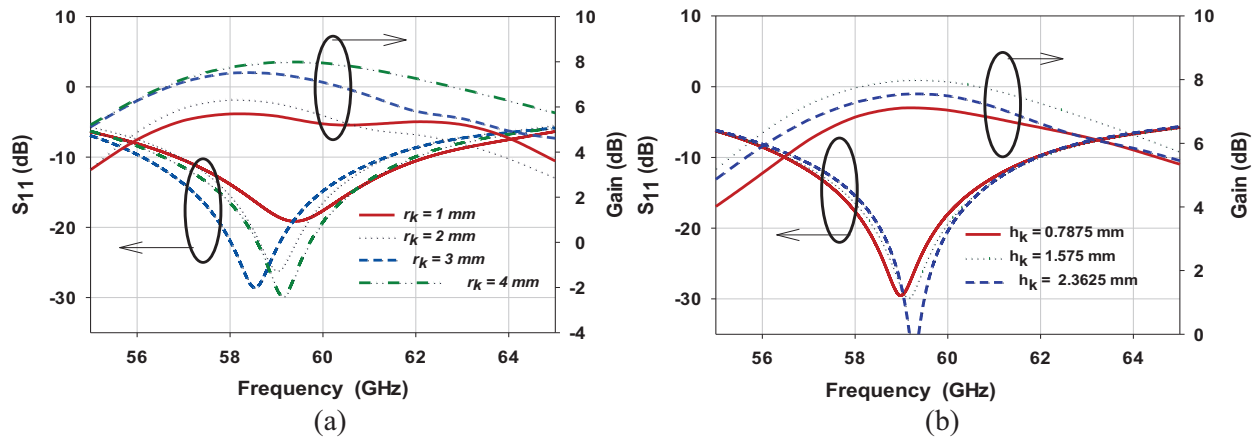


Fig. 2. The simulated antenna's gain and return loss $|S_{11}|$ of the patch antenna with air-cavity: (a) considering the effect of varying the radius of the air cavity (r_k), and (b) the height (h_k).

Figure 3 shows wave propagation comparison between an air cavity with a convex end lens as opposed to one with a flat end lens. The propagating wave of the patch antenna is more focused for the convex-end cavity. In other words, the diffraction angle θ_C of the convex end is less than the diffraction angle θ_F of the flat end. Furthermore, the convex shape of the lens provides the appropriate phase distribution to focus the radiating wave at the desired distance.

Figure 4 shows time snapshots of the electric field generated by CST. The snapshots show six travelling guided wavelengths (λ_{g2}) for three cases: (a) without an air cavity, (b) for a cylindrical air cavity with flat ends, and (c) for a cylindrical air cavity with a convex end. The snapshots show that

the combination of the spherical lens and cylindrical air cavity with convex end has increased the focus of the propagating wave caused by the convex shape of the lens. The cylindrical air cavity under the dielectric lens concentrates the planar wave into a narrow beam. The wave propagation illustrates inside the cavity with different phases are shown in Fig. 4. It can be noticed that the cavity with flat end is less efficient in wave concentration on the focal point (patch antennas) where the focus width $W_F > W_{NC} > W_C$. Therefore, the air cavity covered with the convex lens shape increases the focus of the radiated waves from the patch antenna. This convex shape also enhances the bandwidth of the antenna, as shown in Fig. 5.

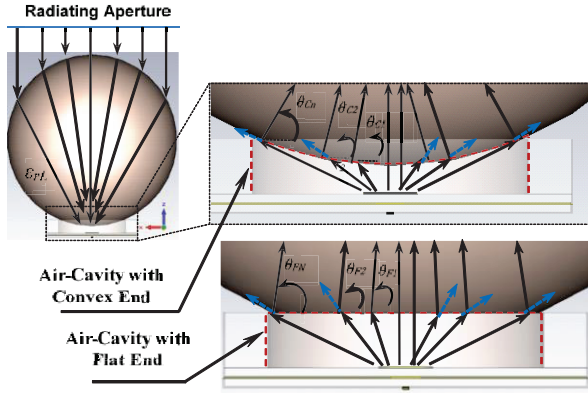


Fig. 3. Illustrates the wave distribution behavior comparison of the air-cavity with a convex end and with a flat end.

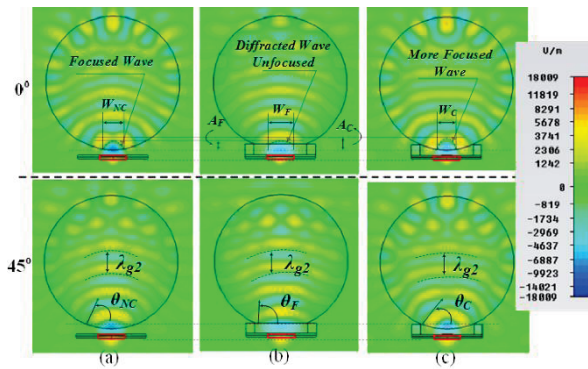


Fig. 4. A time snapshot of the electric field for three cases when the patch antenna fed the lens: (a) without an air cavity, (b) a cylindrical air cavity with flat ends, and (c) a cylindrical air cavity with a convex end.

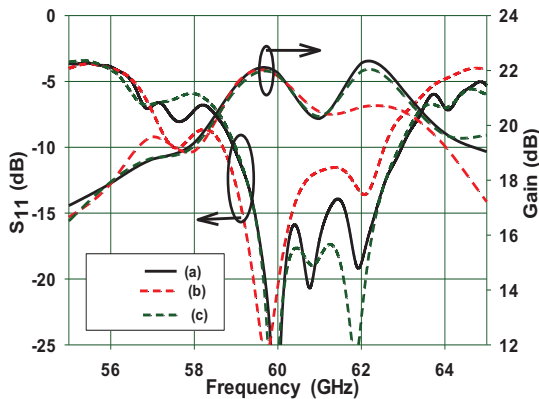


Fig. 5. The simulated antenna's gain, and the return loss $|S_{11}|$ of three cases: (a) without an air cavity, (b) a cylindrical air cavity with flat ends, and (c) a cylindrical air cavity with convex end.

2. Focal point distance d_L

The space between the lens end surface and the patch antenna d_L is a distance associated with the height of the air cavity h_k . After calculating the value of d_L using equation (4) as a starting value, the optimized value has been obtained using CST. The value of d_L was selected to ensure that the focal spot appears on the patch antenna's level.

Figure 6 demonstrates the effect of variation in the d_L on the input reflection coefficient and the antenna gain. In Fig. 6, $|S_{11}|$ responses for the last two values of d_L , 1.75 mm and 2.25 mm, are almost identical and $d_L = 0.75$ mm is selected since it gives a higher average gain over the ISM band. The simulated radiation efficiency of the proposed antenna is 93 percent at 60 GHz, and 88 percent at 63 GHz.

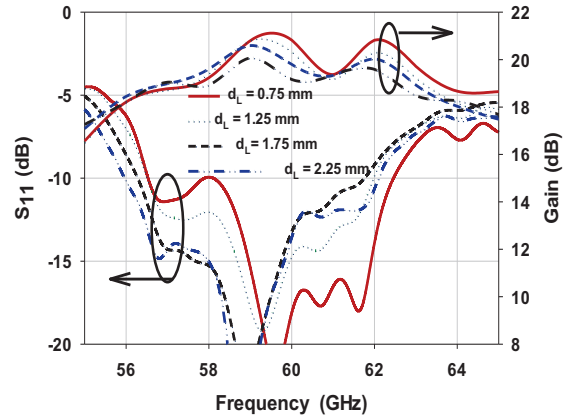


Fig. 6. The simulated reflection coefficient and gain of the proposed antenna, which results from varying the end surface of the lens and the patch (d_L).

IV. EXPERIMENTAL RESULTS

A. Fabrication procedure for the proposed antenna

A standard milling machine with low-cost PCB processes was used to fabricate the two layers slot-coupled patch antenna as well the third layer cavity and the lens holder. The copper thickness of the substrate is $35\mu\text{m}$ with a conductivity $\sigma = 5.80 \times 10^7$ S/m. A photograph of the fabricated prototype is shown in Fig. 7. The antenna layers are manually attached using a thin film of bonding material and are correctly aligned to ensure that the feed line, the aperture slot, and the patch are in their positions.

As shown in Fig. 1, additional length from Ref1 to Ref2 was necessary to create a large enough ground plane for the SouthWest V-connector (1.85

mm connector). In addition, and as shown on the right side of Fig. 7, a circular shaped gap was drilled through the first layer to insert the screws of the V-connector. The 12.7 mm radius spherical dielectric lens is made of polymethyl methacrylate PMMA (Acrylic) material, a lightweight transparent thermoplastic with $\epsilon_{rL} \approx 2.57$, $\tan\delta \approx 0.0032$ at 24 GHz, and $\epsilon_{rL} \approx 2.61$, $\tan\delta \approx 0.002$ at 71 GHz [16]. According to the dielectric constant of the lens material given in [16], the interpolated value of the dielectric constant at 60 GHz is $\epsilon_{rL} \approx 2.6$, $\tan\delta \approx 0.0026$.

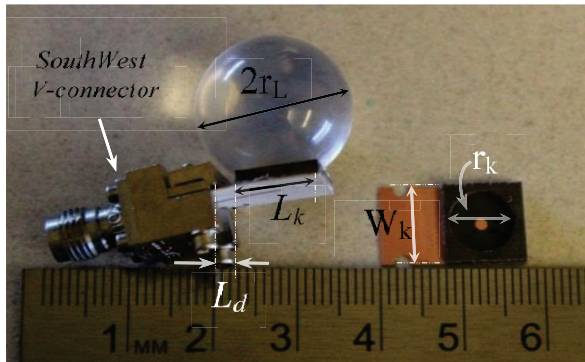


Fig. 7. Photographs of the lens antenna with the circular microstrip patch, fed with the holder substrate.

B. Measurement of the reflection coefficient

The measurements of the reflection coefficient (S_{11}) for the proposed antenna are done using Anritsu 37397C Vector Network Analyzer and Anritsu 3680V 60 GHz Universal Test Fixture. The reflection coefficient measurements were performed with the through-reflect-line (TRL) calibration kit, instead of the standard coaxial line calibration. The TRL calibration technique is a more accurate way to determine precise values for the reflection coefficient, especially for the MMW band, where any inaccurate connection during the measurements could cause inaccurate results for measured antenna parameters [17].

Figure 8 compares the measured reflection coefficient and antenna gain with CST results for two antenna configurations of the radiated element with and without the lens. The measured impedance bandwidth (≤ -10 dB) is 3.5 GHz corresponds to 5.84% at 60 GHz. In the measured result of $|S_{11}|$, there is a shift in resonant frequency compared with CST results – this may be caused by inaccuracy in

the substrate material properties at 60 GHz and/or by the effects of etching and alignment tolerances in the fabrication process. The material used in the simulation for the microstrip feed line is RO6010, and the patch's substrate is RO5880. Dielectric constants of both substrates are slightly different at 60 GHz, from those specified by the manufacture at 10 GHz. As noted in Fig. 8, the measured and calculated reflection coefficient of the proposed antenna responses are fluctuating due to exciting multi-high order modes resonated in the air-cavity, which results in a 3-4 dB gain variation.

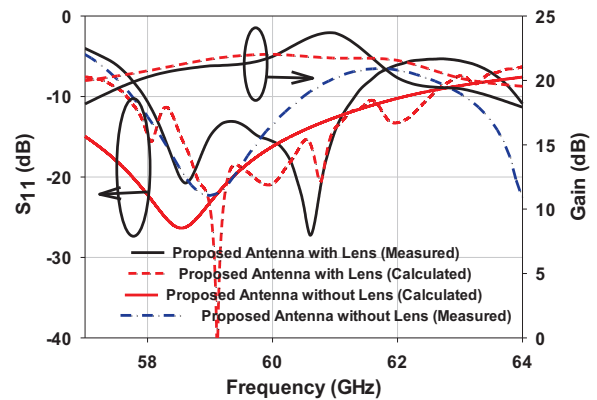


Fig. 8. Measured and calculated reflection coefficient of the proposed antenna.

C. Radiation pattern

The radiation patterns within the bandwidth range (from 58 GHz to 61 GHz) are measured in an anechoic chamber. As shown in Fig. 9, the E-plane is the yz -plane, and the H-plane is xy -plane. Two prototypes are measured: the first is the radiating element (a circular patch with cavity), and the second is the proposed antenna (a lens mounted on the radiating element). In both cases, the radiation pattern is measured with the antennas directly mounted by a 1.85 mm South-West Microwave connector.

The measured and calculated E- and H-planes radiation patterns for the patch antenna with the holder only (no lens) within the ISM frequency band at 58 GHz to 61 GHz are shown in Fig. 10. Both the CST and measured results agree well within the main lobe and HPBW range. In the results, the back lobe radiation of both the E- and H-planes was higher than expected due to the small ground plane and strong resonance. Furthermore, a higher side lobe level (SLL) within an angle range

of 150° to 270° , the side of the setup and the antenna's connector was observed for the measured E-plane pattern.

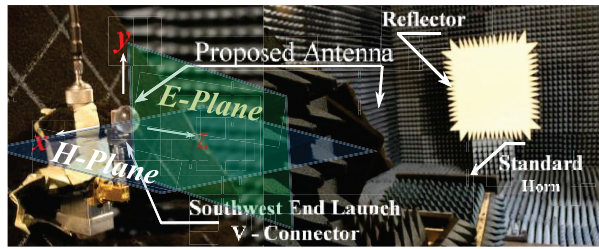


Fig. 9. Setup for radiation pattern measurements.

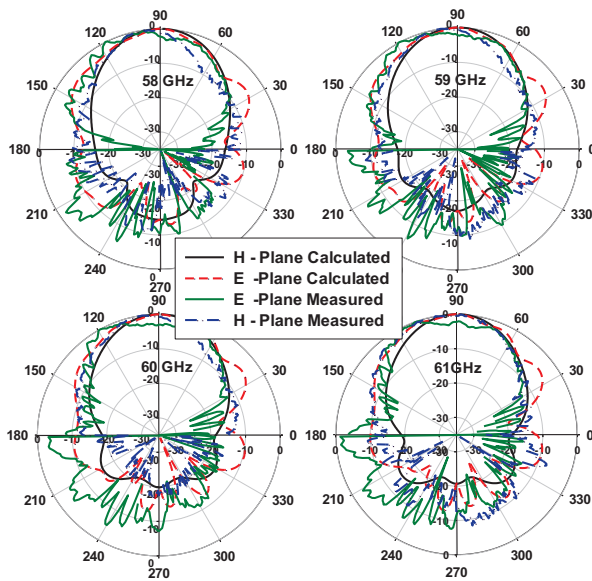


Fig. 10. The normalized E- and H-plane co-polarization patterns of the circular patch with holder for 58 GHz - 61 GHz.

In Fig. 11, the measured and the calculated results of the far-field patterns are presented for both the E- and H-planes of the proposed antenna, at 58 GHz to 61 GHz. The HPBW of the measured results agreed with the CST results for the entire ISM band. Moreover, the measured results of the H-plane agree quite well with the calculated results. However, the SLL in the measured results of the E-plane is higher than expected. This is mainly due to the effect the antenna's setup and the reflection from cable and connectors. The high reflection is caused by the Southwest connector, which is perpendicular to the E-plane, as seen in Fig. 9. A large reflection from the lab setup is also affecting

the side lobes in Fig. 11, especially from the feed line side. Meanwhile, the radiation pattern in the H-plane is far from the connectors, and thus the measured results of the radiation pattern agree well with CST results. Therefore, in a practical deployment of this antenna, this effect would not appear when mounted using a proper packaging system. This high gain hybrid antenna is a good alternative candidate to array structure for some applications such as mine wireless communications [19]. In addition, it could also be used as an array element taken into account the spacing between the elements and a proper lens diameter to fit in the array and avoid grating lobes. The estimated radiation efficiency from the measured gain and directivity is greater than 90 percent at 60 GHz, and it is 85 percent at 64 GHz.

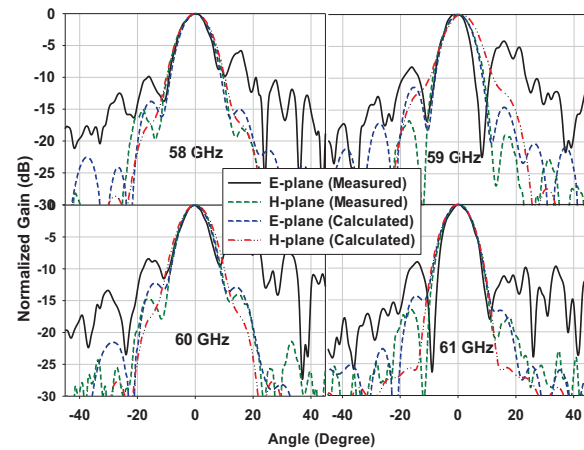


Fig. 11. Normalized E- and H-plane patterns of the proposed antenna at 58 GHz - 61 GHz.

V. CONCLUSION

A circular patch slot-fed antenna loaded with a dielectric lens, optimized for operation at 60 GHz, is successfully implemented. An air cavity holder provides a noticeable enhancement, and makes the spherical dielectric lens simple to mount on the antenna. This prototype achieves a high measured gain of ~ 20 dB along the ISM band. The antenna impedance bandwidth is 3.5 GHz within the ISM unlicensed band. The proposed low cost antenna with a simple structure and a small size of $12.412 \times 10.5 \times 27.553$ mm³ would be useful and suitable for millimeter-wave band applications, especially for imaging and mining applications. Moreover, the antenna can fit into portable devices.

REFERENCES

- [1] E. E. Altshuler and R. A. Meir, "A comparison of experimental and theoretical values of atmospheric absorption at the longer millimeter wavelengths," *IEEE Trans. Antennas Propagat.*, vol. AP-36, no. 10, pp. 1471-1480, Oct. 1988.
- [2] A. Perron, T. A. Denidni, and A. R. Sebak, "High-gain hybrid dielectric resonator antenna for millimeter-wave applications: design and implementation," *IEEE Trans. Antennas Propagat.*, vol. 57, no. 10, pp. 2882, 2009.
- [3] E. Ayman and A. Sebak, "High-gain hybrid microstrip/conical horn antenna for MMW applications," *IEEE Antennas and Wireless Propagation Letters*, vol. 11, pp. 129-132, 2012.
- [4] C. Karnfelt, P. Hallbjorner, H. Zirath, and A. Alping, "High gain active microstrip antenna for 60-GHz WLAN/WPAN applications," *IEEE Trans. Microw. Theory Tech.*, vol. 54 (6), pp. 2593-2603, 2006.
- [5] X. Wu, G. V. Eleftheriades, and T. E. van Deventer-Perkins, "Design and characterization of single- and multiple-beam mm-wave circularly polarized substrate lens antennas for wireless communications," *IEEE Trans. Microw. Theory Tech.*, vol. 49, no. 3, pp. 431-441, 2001.
- [6] Y. Larry, M. Shoucri, and P. Moffa, "Passive millimeter wave imaging," *IEEE Microwave Magazine*, vol. 4.3, pp. 39-50, 2003.
- [7] J. Hasch, E. Topak, R. Schnabel, T. Zwick, R. Weigel, and C. Waldschmidt, "Millimeter-wave technology for automotive radar sensors in the 77 GHz frequency band," *IEEE Trans. Microw. Theory Tech.*, vol. 60, no. 3, pp. 845-860, 2012.
- [8] T. H. Buttgenbach, "An improved solution for integrated array optics in quasioptical mm and submm receivers: the hybrid antenna," *IEEE Trans. Microw. Theory Tech.*, vol. 41, no. 10, pp. 1750-1761, 1993.
- [9] D. Lemaire, C. A. Fernandes, P. Sobieski, and A. Barbosa, "A method to overcome the limitations of G.O. in axis-symmetric dielectric lens shaping," *Int. J. Infrared and MMW*, vol. 17, no. 8, pp. 1996.
- [10] H. Kao-Cheng, "Millimeter wave lens antennas," *Modern Lens Antennas for Communications Engineering*, pp. 113-146, 2013.
- [11] H. Kaouach, L. Dussopt, J. Lanteri, T. Koleck, and R. Sauleau, "Wideband low-loss linear and circular polarization transmit-arrays in V-band," *IEEE Trans. Antennas Propagat.*, vol. 59, no. 7, pp. 2513-2523, 2011.
- [12] A. Henderson, A. E. England, and J. R. James, "New low-loss millimeter wave hybrid microstrip antenna array," *Eleventh European Microwave Conference*, Amsterdam, The Netherlands, 1981.
- [13] M. Al Henawy and M. Schneider, "Planar antenna arrays at 60 GHz realized on a new thermoplastic polymer substrate," *Proceedings of the Fourth European Conference on Antennas and Propagation (EuCAP)*, pp. 1-5, 2010.
- [14] L. Mall and R. B. Waterhouse, "Millimeter-wave proximity-coupled microstrip antenna on an extended hemispherical dielectric lens," *IEEE Trans. Antennas Propagat.*, vol. 49, no. 12, pp. 1738-1749, 2001.
- [15] N. T. Nguyen, A. Rolland, A. V. Boriskin, G. Valerio, L. LeCoq, and R. Sauleau, "Size and weight reduction of integrated lens antennas using a cylindrical air cavity," *IEEE Trans. Antennas Propagat.*, vol. 60, no. 12, pp. 5993-5998, 2012.
- [16] W. J. Lamb, "Miscellaneous data on materials for millimeter and submillimetre optics," *Int. J. Infrared Millimeter Waves*, vol. 17, no. 12, 1996.
- [17] R. B. Marks, et al., "Characteristic impedance determination using propagation constant measurement," *IEEE Microwave Guided Wave Let.*, vol. 1, pp. 141-143, 1991.
- [18] E. Vilar and K. W. Wan, "Narrow and wide band estimates of field strength for indoor communications in the millimetre band," *Electronics Division Colloquium on Radiocommunications in the Range 30-60 GHz*, pp. 5/1-5/8, Jan. 17, 1991.
- [19] I. Ben Mabrouk, J. Hautcoeur, L. Talbi, M. Nedil, and K. Hettak, "Feasibility of a millimeter-wave MIMO system for short-range wireless communications in an underground gold mine," *IEEE Trans. Antennas Propagat.*, vol. 61 (8), pp. 4296-4305, 2013.
- [20] H. Kaouach, L. Dussopt, J. Lanteri, T. Koleck, and R. Sauleau, "Wideband low-loss linear and circular polarization transmit-arrays in V-

band,” *IEEE Trans. Antennas Propag.*, vol. 59, no. 7, pp. 2513-2523, 2011.

- [21] S. Raman and G. M. Rebeiz, “Single and dual polarized millimeter wave slot ring antennas,” *IEEE Trans. Antennas Propag.*, vol. 44, no. 11, pp. 1438-1444, Nov. 1996.
- [22] T. H. Büttgenbach, “An improved solution for integrated array optics in quasioptical mm and submm receivers: the hybrid antenna,” *IEEE Trans. Microw. Theory Tech.*, vol. 41, no. 10, pp. 1750-1761, Oct. 1993.
- [23] J. J. Lee, *Lens Antennas, Microwave Passive and Antenna Components*, in *Handbook of Microwave and Optical Components*, K. Chang Ed., New York: Wiley, vol. 1, ch. 11.2, pp. 595-625, 1989.



Zouhair Briqech received the B.Sc. degree in Communications Engineering from High Institute of Electrical and Electronics Engineering, Bani-Walid, Libya, in 2003, and the M.Sc. degree in Communications and Microwave Engineering from Academy of Graduate studies, Tripoli, Libya, in 2007. In 2010, he joined to the Microwave group of Department of Electrical and Computer Engineering, Concordia University, as a Researcher Assistant and he is now working towards his Ph.D. degree.



Abdel-Razik Sebak received the B.Sc. degree in Electrical Engineering from Cairo University in 1976, and the M.Eng. and Ph.D. degrees from the University of Manitoba in 1982 and 1984, respectively. From 1984 to 1986, he was with the Canadian

Marconi Company. From 1987 to 2002, he was a Professor of Electrical and Computer Engineering, University of Manitoba. He is currently a Professor of Electrical and Computer Engineering, Concordia University. His current research interests include phased array antennas, computational electromagnetics (EM), integrated antennas, EM theory, interaction of EM waves with new materials, and bio-EM. Sebak received the 1992 and 2000 University of Manitoba Merit Award for outstanding Teaching and Research, the 1994 Rh Award for Outstanding Contributions to Scholarship and Research in the Applied Sciences category, and the 1996 Faculty of Engineering Superior Academic Performance. He has served as Chair for the IEEE Canada Awards and Recognition Committee (2002-2004).



Tayeb A. Denidni received the B.Sc. degree in Electronic Engineering from the University of Setif, Setif, Algeria, in 1986, and the M.Sc. and Ph.D. degrees in Electrical Engineering from Laval University, Quebec, Canada, in 1990 and 1994, respectively. From 1994 to 2000, he was a Professor with the Engineering Department, Université du Québec, Rimouski, Quebec, Canada. Since August 2000, he has been a Professor with Institut National de la Recherche Scientifique (INRS), Université du Québec, Montreal, Canada. He is leading a large research group consisting of two research scientists, five Ph.D. students, and three M.S. students. Over the past 10 years, he has graduated numerous graduate students. His current research interests include planar microstrip filters, dielectric resonator antennas, EM-bandgap antennas, antenna arrays, and microwave and RF design for wireless applications. He has authored over 100 papers in refereed journals. He has also authored or co-authored over 140 conference papers.